Electronic Supplementary Material (ESI) for CrystEngComm.

Electronic Supplementary Information

Unexpected solution phase formation of hollow PtSn alloy nanoparticles from Sn deposition on Pt dendritic structures.

Taehyun Kwon,†[b] Jongsik Park,†[a,b] Hionsuck Baik,[c] Seoin Back,[d] Bartoz Błasiak,[a,b] Minhaeng Cho,[a,b] Yousung Jung,[d]*and Kwangyeol Lee[a,b]*

[a] *Center for Molecular Spectroscopy and Dynamics, Institute for Basic Science (IBS), Seoul 02841, Republic of Korea, E-mail: kylee1@korea.ac.kr*
[b] *Department of Chemistry, Korea University, Seoul 02841, Republic of Korea.*
[c] *Korea Basic Science Institute (KBSI), Seoul 02841, Republic of Korea*
[d]*Graduate School of EEWS, Korea Advanced Institute of Science and Technology (KAIST), 291 Daehakro, Daejeon 34141, Korea, E-mail: ysjn@kaist.ac.kr*

†These authors contributed equally.

Material Characterizations

Transmission electron microscopy (TEM) and high-resolution TEM were performed on a TECNAI G2 20 S-Twin operated at 200 kV and TECNAI G2 F30 operated at 300 kV. Elemental mapping and energy dispersive X-ray spectra (EDX) were obtained with a FEI Titan Cubed 60-300 with Chemi-STEM technology and a JEOL ARM200F Cs STEM. Powder X-ray diffraction (PXRD) patterns were collected with a Rigaku Ultima III diffractometer system using a graphite-monochromatized Cu-Kα radiation at 40 kV and 30 mA

Experimental Section

Reagents

$Pt(acac)_2$ (platinum(II) acetylacetonate, 97%), $Sn(OAc)_2$ (tin(II) acetate), 1,2-hexadecanediol (1,2-HDD, 90%), oleic acid (90%), and oleylamine (98%) were purchased from Sigma-Aldrich. All reagents were used as received without further purification.

Preparation of hollow PtSn nanoparticles (HPSN)

A slurry of $Pt(acac)_2$ (0.015 mmol, 5.9 mg), 1,2-hexadecanediol (0.12 mmol, 31.0 mg), oleic acid (3 mmol), and oleylamine (12 mmol) was prepared in a 100 mL Schlenk tube equipped with magnetic stirrer. The tube was placed in an oil bath which was preheated to 80 ^{o}C for 5 min and then evacuated for 5 min with a magnetic stirring at that temperature, and finally purged with 1 atm Ar gas. The tube was then directly placed in a hot oil bath, which was preheated to 270 ^{o}C and kept at that temperature for 30 min under Ar condition. After 30 minutes, a mixture of $Sn(OAc)_2$ (0.015 mmol, 3.6 mg) and oleylamine (3 mmol) was added to the reaction mixture *via* syringe, and kept at that temperature for another 60 min. Finally, dark black precipitates could be obtained by cooling down the solution to room temperature and then by centrifugation with added toluene and methanol (v/v = 15/20).

Calculation Method

Electronic energies were calculated using the Vienna Ab initio Simulation Package (VASP)[S1-S2] with the RPBE exchange functional[S3-S4] and projector-augmented wave pseudopotential.[5] A cut-off energy for plane wave basis set was set to 500 eV and k-points were sampled using the (3×3×1) and (4×3×1) Monkhorst-Pack mesh for Pt (100), Pt (111) and Pt (211) surfaces, respectively.[6] The electronic energies of Pt and Sn bulk crystal were calculated with (9×9×1) Monkhorst-Pack mesh. Five-layered

Pt slabs were modeled using (3×3) surface unit cell for all surfaces containing 45 atoms in total. The bottom two Pt layers were fixed to their bulk positions, and all other Pt atoms and adsorbates were relaxed until the total forces on them were less than 0.05 eV/Å.

For a substitution reaction, $Sn_1 + Pt_n(hkl) \rightarrow [Pt_{n-1}(hkl)+Sn_1] + Pt_1$, the substitution energy, E_{sub}, was calculated as follows:

$$E_{sub} = E[Pt_{n-1}(hkl)+Sn_1] + E[Pt_1] - E[Sn_1] - E[Pt_n(hkl)]$$

where $E[Pt_{n-1}(hkl)+Sn_1]$ and $E[Pt_n(hkl)]$ are electronic energies of Sn-substituted slab and pure Pt slab, and $E[Pt_1]$ and $E[Sn_1]$ are electronic energies of Pt and Sn atoms referenced to their bulk crystal states. Based on the lowest Esub, which corresponds to Sn substitution to the 1st layer of Pt (100), the relative substitution energies ($\Delta E_{sub} = E_{sub} - E_{sub}$[1st layer, Pt (100)]) were obtained and shown in Fig. 4 and Fig. S9.

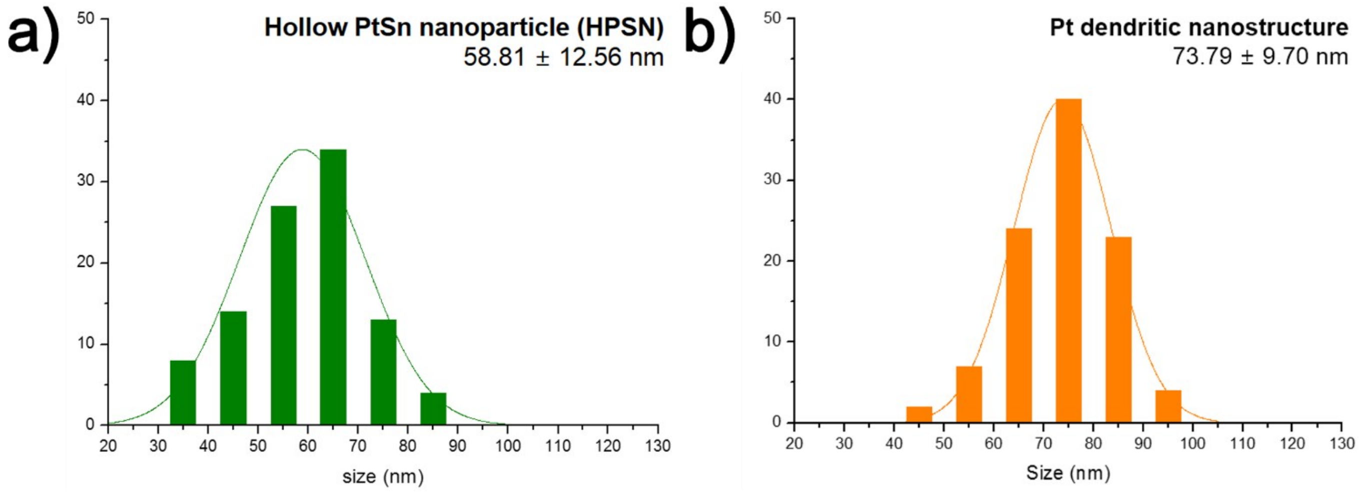

Fig. S1. Size distribution histograms of (a) HPSN and (b) Pt dendritic nanostructures. The average size of the HPSN and Pt dendritic nanostructures are 58.81±12.56 nm and 73.79±9.70 nm, respectively. The size of particles decreased after Sn precursor injection.

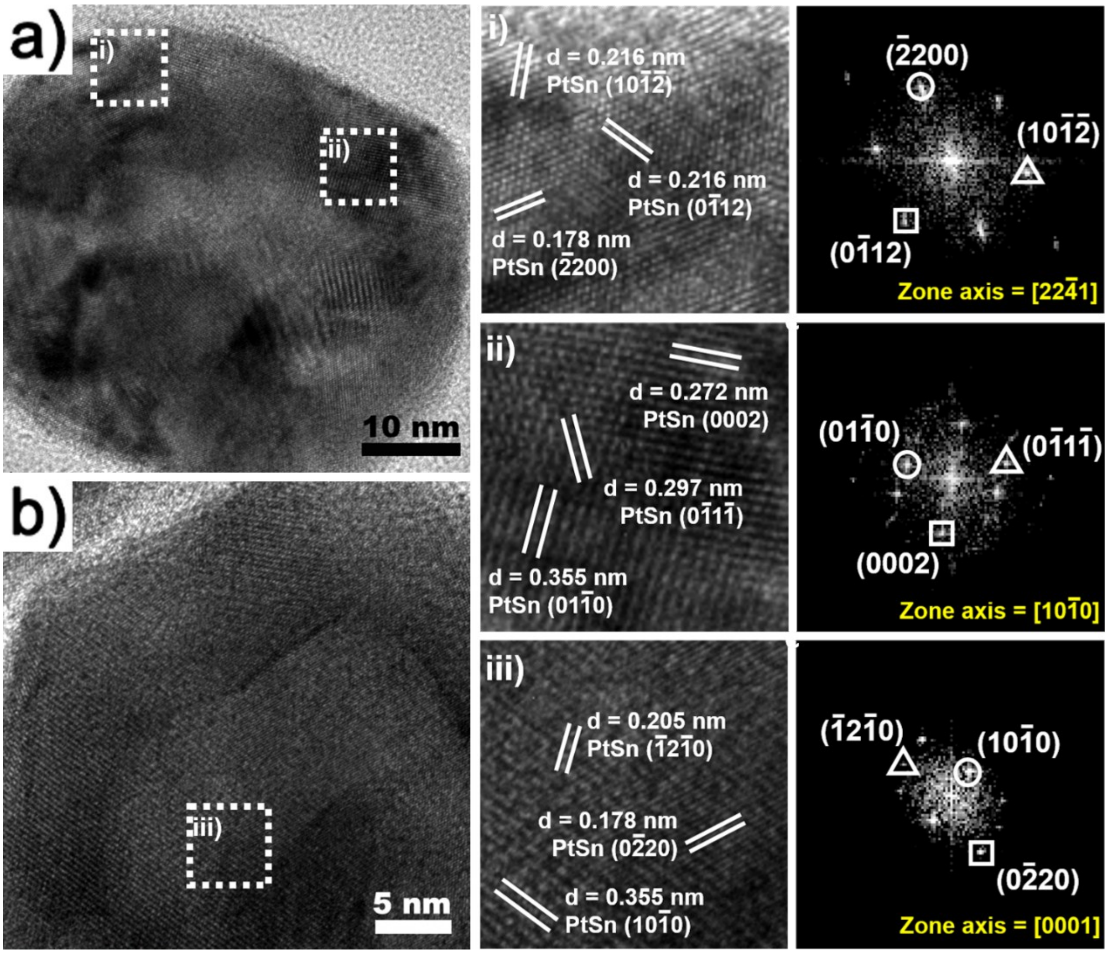

Fig. S2. HRTEM images of HPSN with various zone axes. (i-ii) Enlarged HRTEM images of (a). (iii) Enlarged HRTEM image of (b) with the zone axis of [0001]. The white solid lines in the image represent the lattice spacings of *hcp* PtSn phase. The zone axes in (i) and (ii) are different, indicating that the resulting HPSN is not single-crystalline.

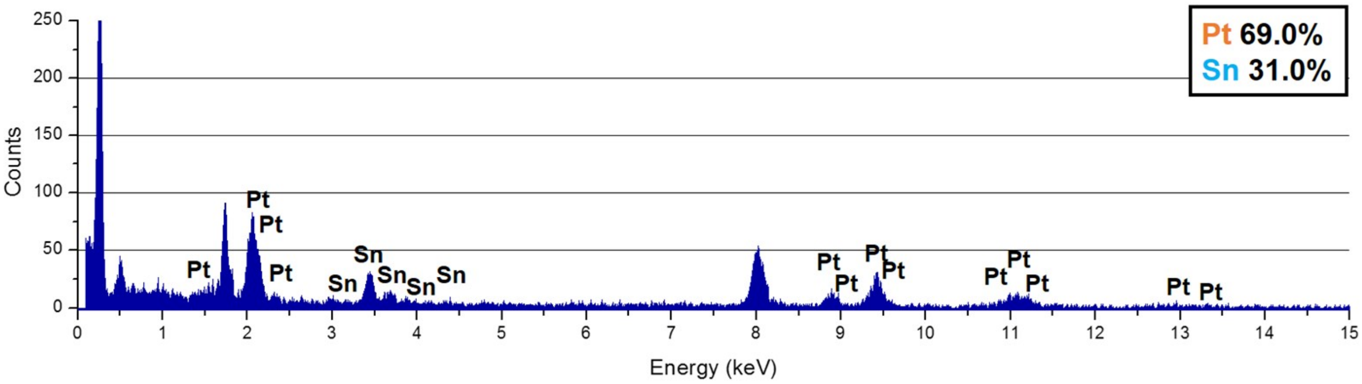

Fig. S3. Energy dispersive X-ray spectra (EDS) of HPSN.

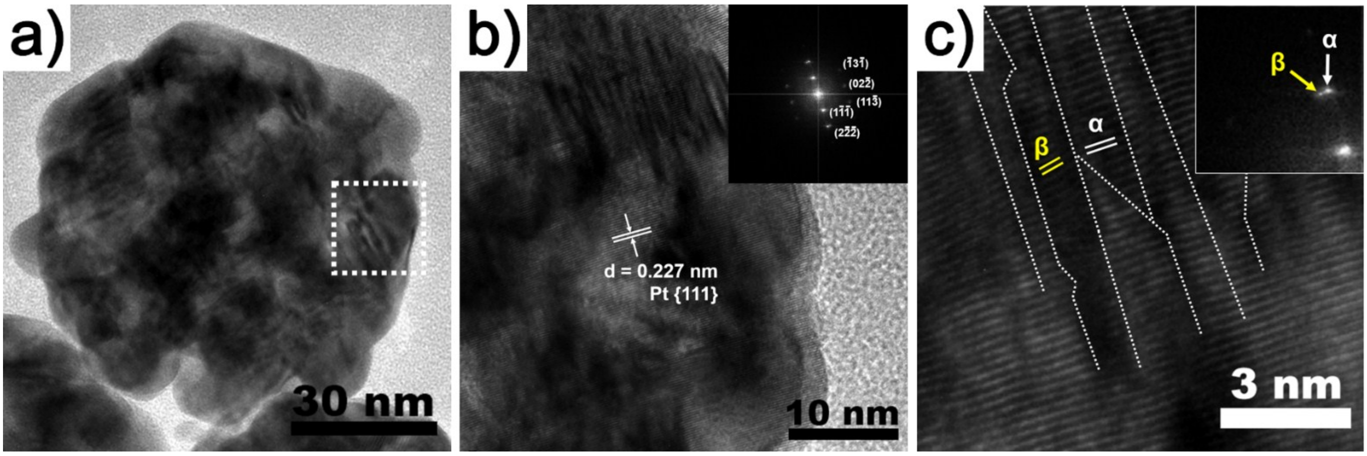

Fig. S4. (a) HRTEM image of Pt dendritic nanostructures. (b) Enlarged HRTEM image and corresponding fast Fourier-transform (FFT) patterns with the zone axis of [211] indicate that the Pt dendritic nanostructures have a *fcc* Pt phase. The white solid lines indicate the lattice spacing of {111} plane of *fcc* Pt phase. (c) Enlarged HRTEM image in Fig. S4b. The white dotted lines indicate the grain boundaries of Pt dendritic nanostructures. While the overall crystal growth directions of constituting arms of a dendritic structure are rather similar, the dendritic nanostructure is definitely not of single-crystalline nature. Furthermore, the arm end surfaces are very poorly defined.

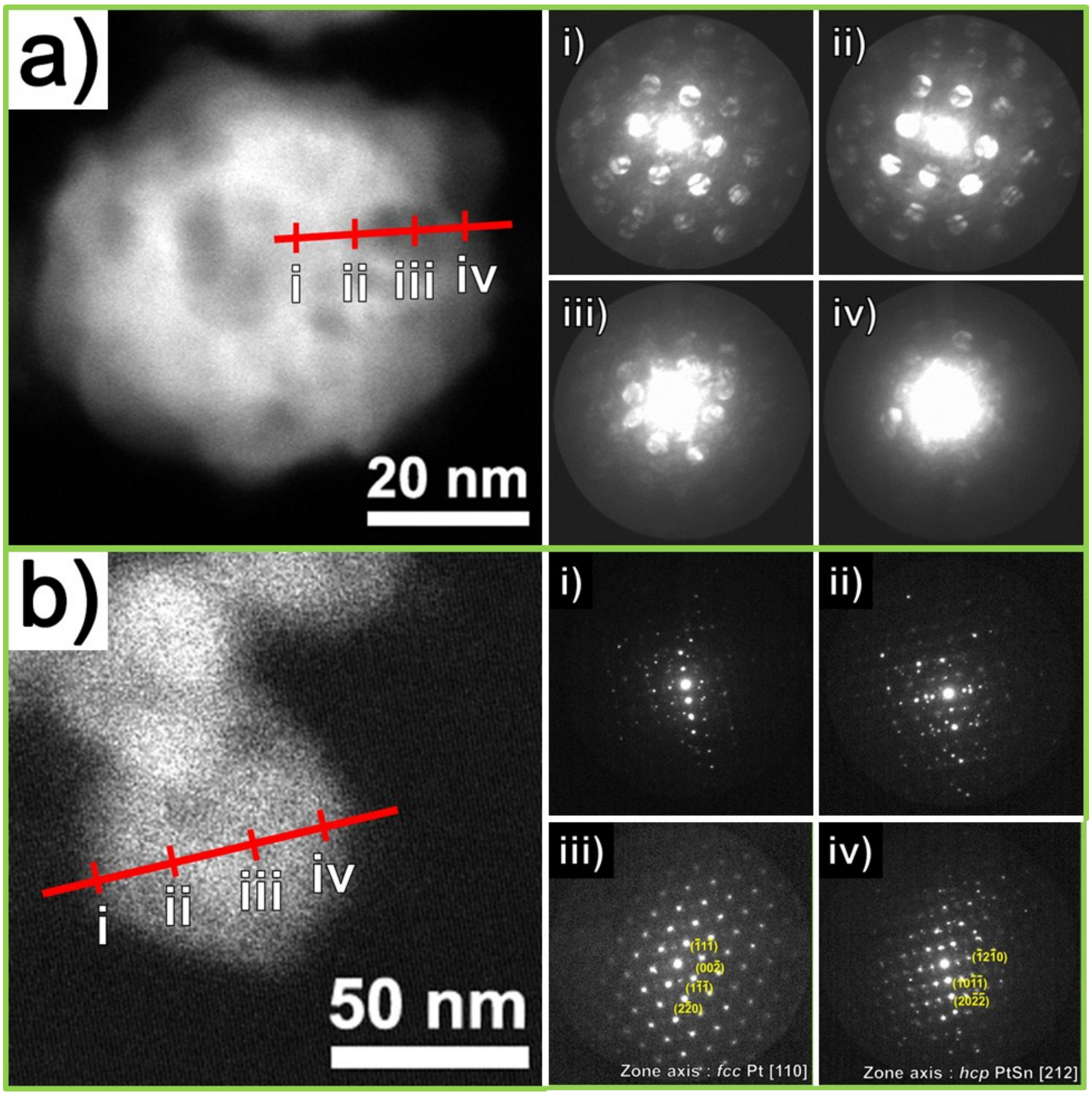

Fig. S5. (a, b) STEM image and its corresponding nanobeam electron diffraction patterns of reaction intermediates after 1 min from injection of Sn precursor (Fig. 2b.). While the diffraction patterns in the core are well developed, the diffraction patterns on the periphery are poorly defined due to the poor crystallinity.

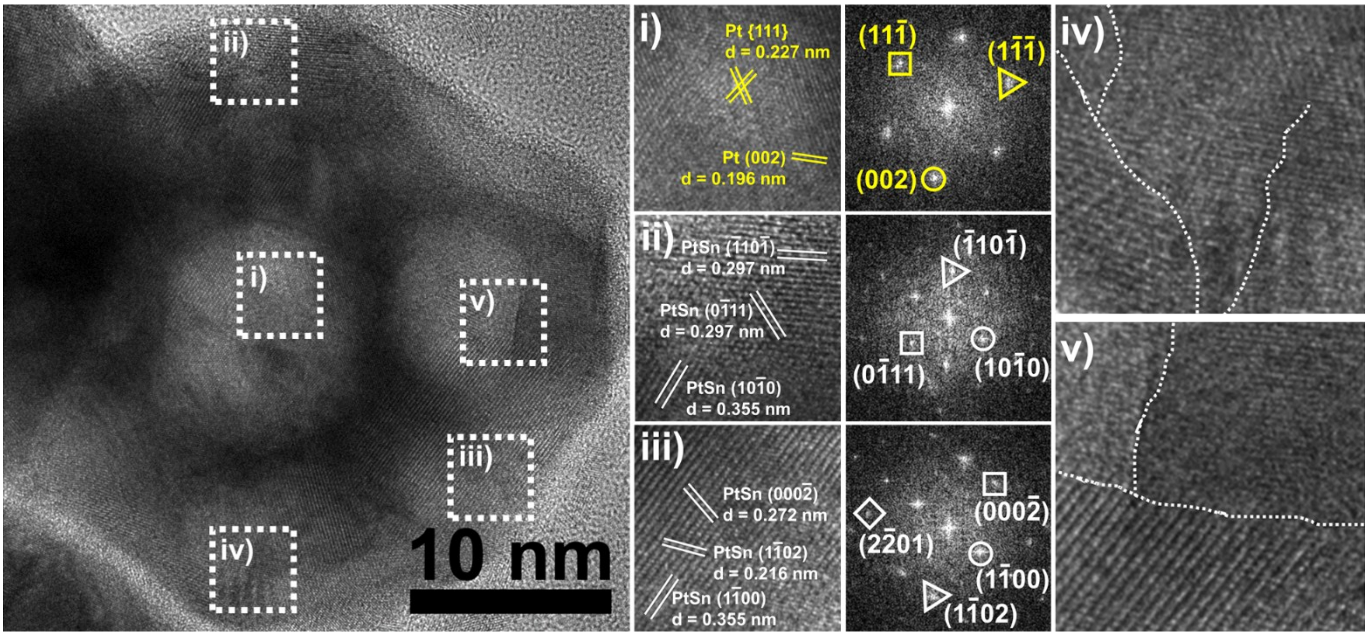

Fig. S6. HRTEM image of reaction intermediates after 1 min from injection of Sn precursor (Fig. 2b.) i) – iii) Enlarged HRTEM images of 1 min reaction intermediates, the yellow and white solid lines represent the lattice spacings of *fcc* Pt and *hcp* PtSn, respectively. The corresponding FFT patterns in i) ~ iii) reveal the zone axes of *fcc* [110], *hcp* [01$\bar{1}$1] and *hcp* [11$\bar{2}$0]. These results indicate the co-existence of *fcc* Pt phase in the core and *hcp* PtSn phase in the shell. iv) – v) Enlarged HRTEM images of 1 min reaction intermediates; the white dotted lines indicate the grain boundaries of the polycrystalline PtSn shell.

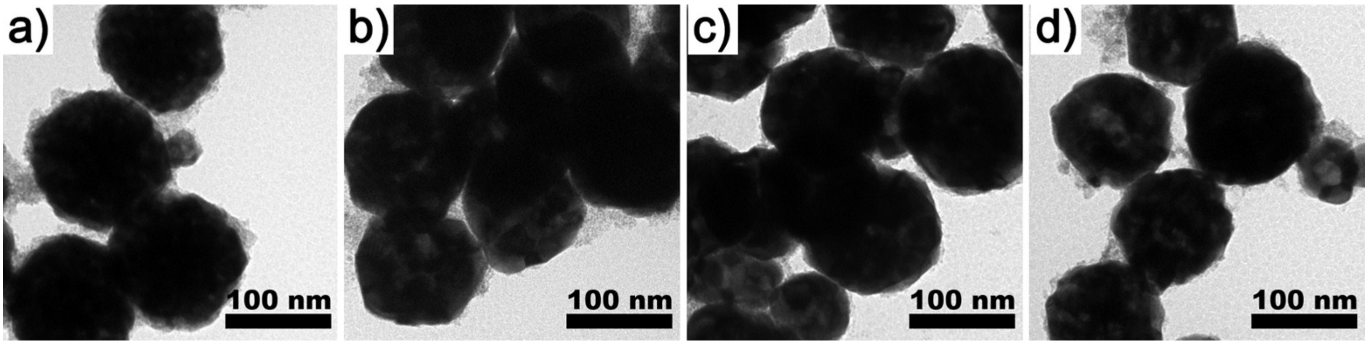

Fig. S7. TEM images of PtSn nanostructures obtained with Sn precursor injected at different temperatures of (a) 230, (b) 240, (c) 250 and (d) 260 ^{o}C.

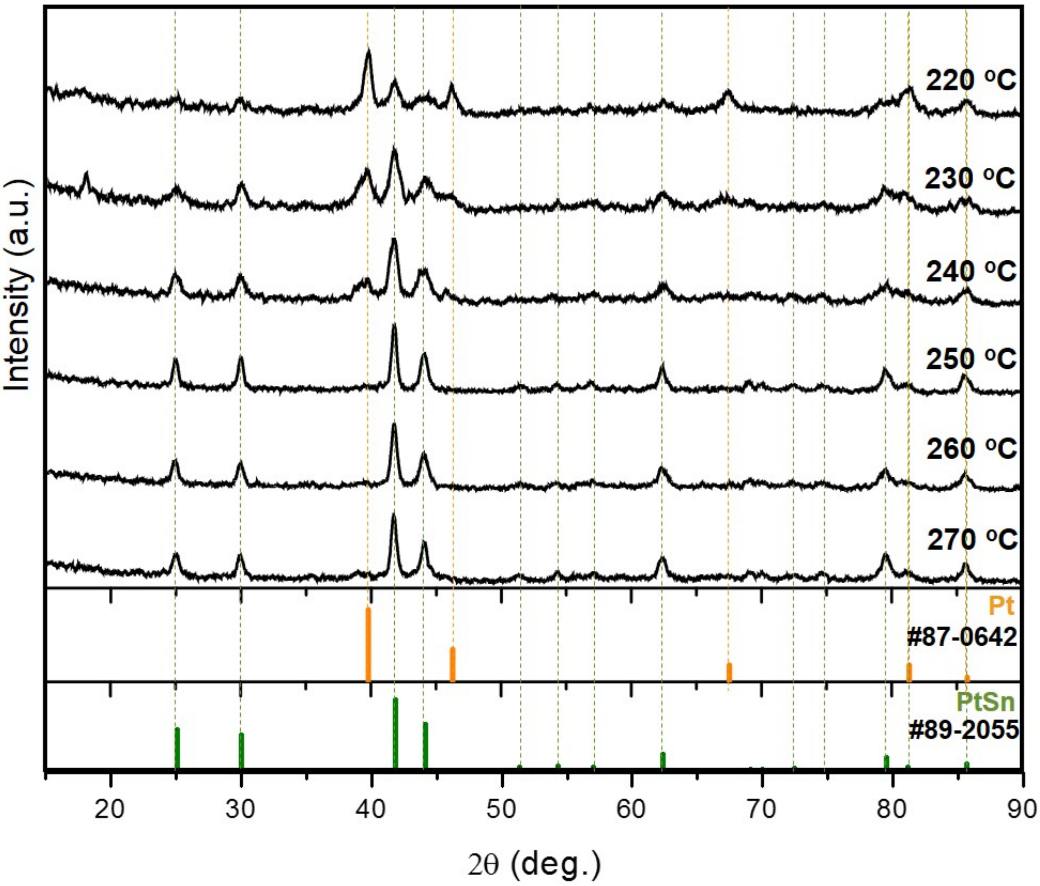

Fig. S8. Powder X-ray diffraction (PXRD) patterns of PtSn nanostructures with Sn precursor injection at different temperatures from 220 °C to 270 °C. The colour sticks indicate the reference X-ray diffraction lines; orange–Pt (JCPDS #87-0642), green–PtSn (JCPDS #89-2055).

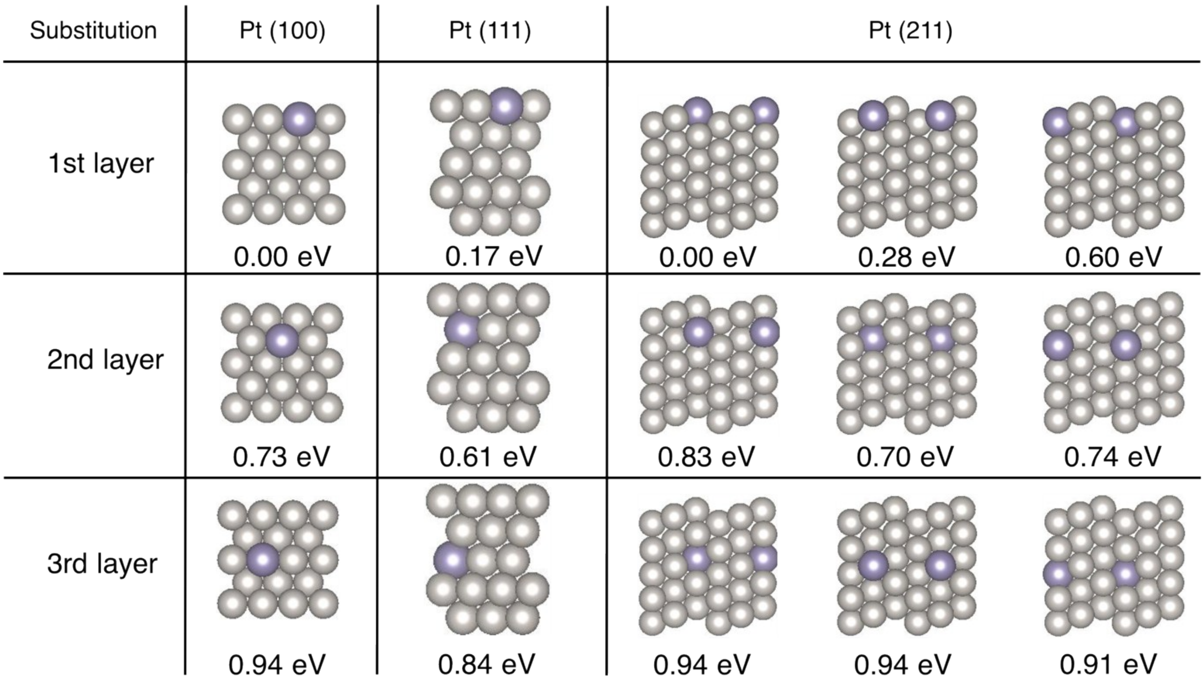

Fig. S9. Side view of the Pt (100), Pt (111) and Pt (211) calculation models, in which grey and blue balls indicate Pt and Sn atoms, respectively. The calculated relative substitution energies (ΔE_{sub}) are shown in reference to the most stable substitution energies (Sn substituted to the 1st layer of Pt (100)).

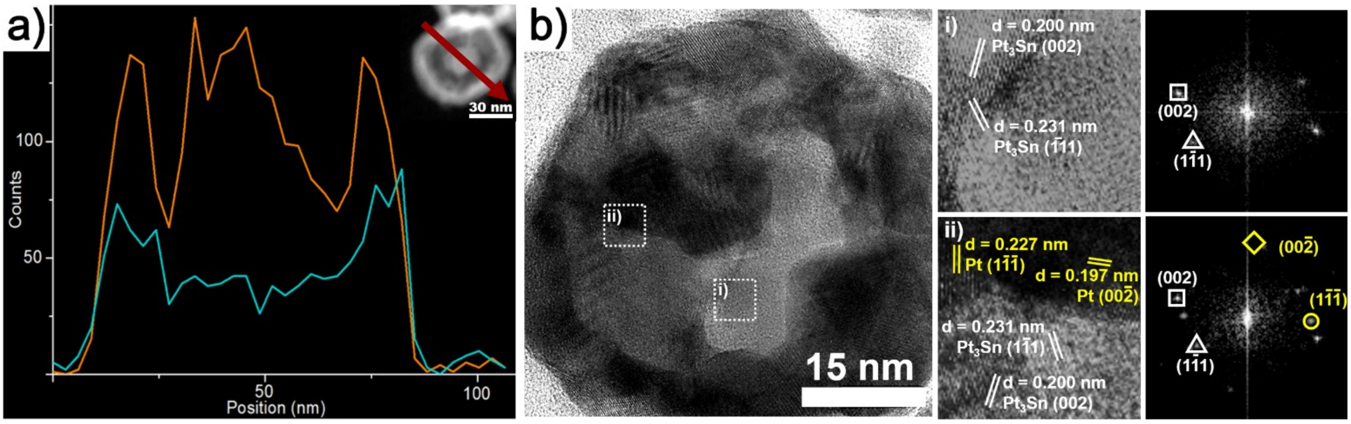

Fig. S10. Structural analysis of yolk-shell Pt-Pt$_3$Sn nanostructure (YPSN). (a) The HAADF-STEM image (inset) and corresponding line profile of YPSN. (b) HRTEM image of YPSN with the zone axis of Pt [110] and Pt$_3$Sn [110]. (i, ii) Enlarged HRTEM images and corresponding FFT patterns of YPSN. The white and yellow solid lines in magnified HRTEM image represent the lattice spacing of *fcc* Pt$_3$Sn phase, and *fcc* Pt phase, respectively. These results indicate that the structure of YPSN consists of Pt yolk and Pt$_3$Sn alloy shell.

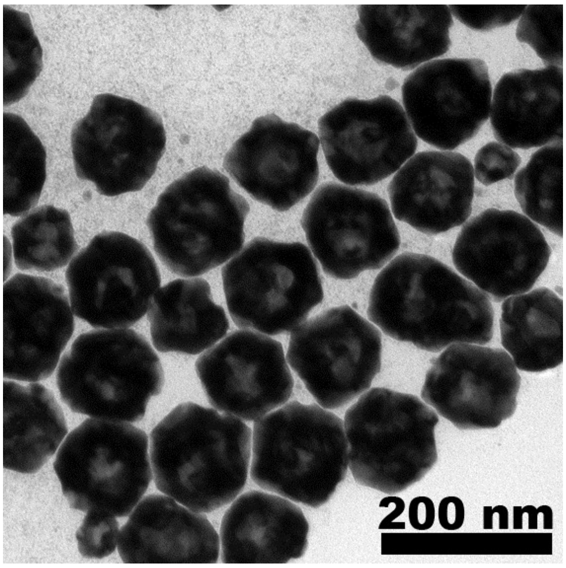

Fig. S11. TEM image of hollow PtSn nanostructures with further injection of Sn precursor (0.67 equiv.) to YPSN; the total amount of injected Sn precursor is now 1 equiv. Further Sn precursor leads to more outward diffusion of Pt atoms from the core, forming hollow nanostructures with a single void.

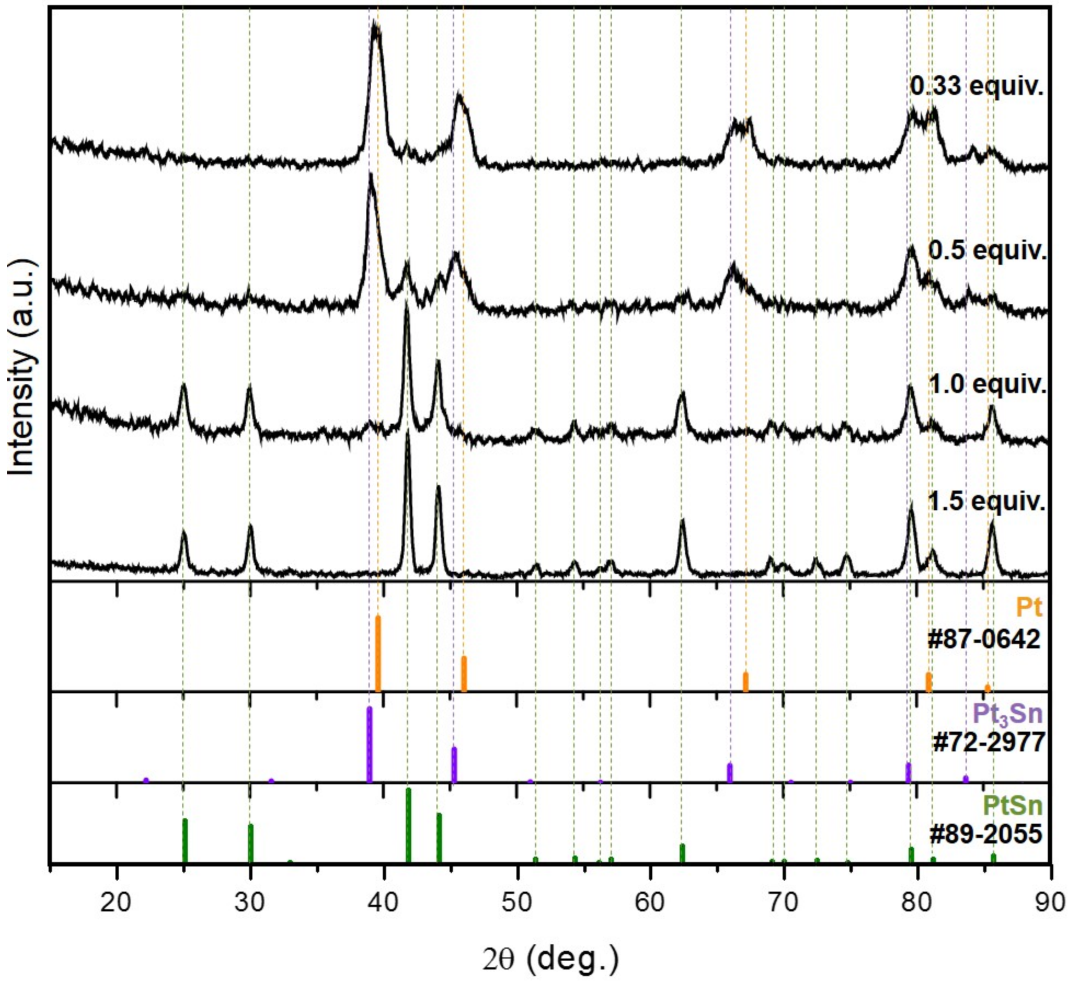

Fig. S12. Powder X-ray diffraction (PXRD) patterns of PtSn nanostructures with 0.33 to 1.5 equiv. Sn precursor. The colour sticks indicate the reference X-ray diffraction lines; orange–Pt (JCPDS #87-0642), purple–Pt_3Sn (JCPDS #72-2977), and green–PtSn (JCPDS #89-2055).

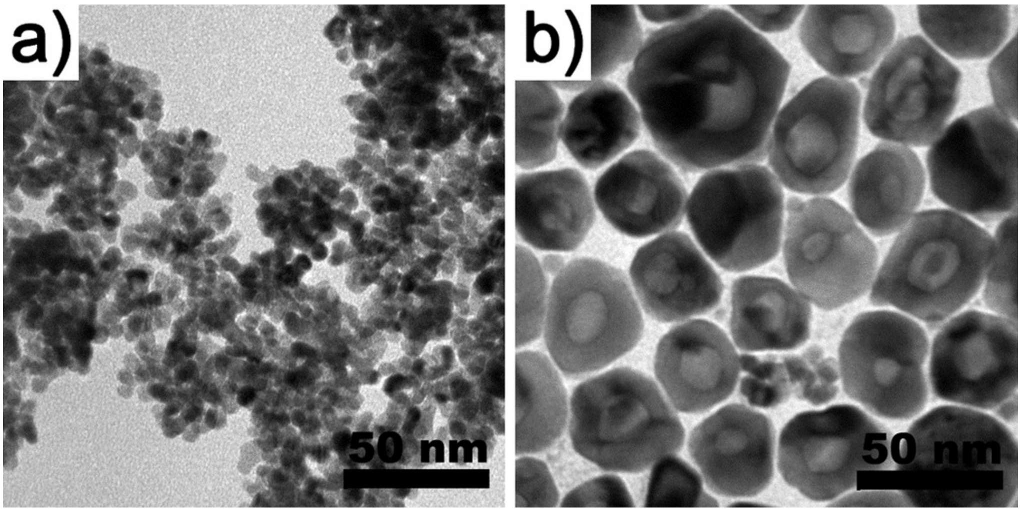

Fig. S13. TEM images of (a) small (40~50 nm) dendritic Pt nanocrystals and (b) hollow PtSn nanocrystals synthesized from small dendritic Pt nanocrystals (Fig. S13a). Smaller dendritic Pt nanocrystals were synthesized with a shorter reaction time (15 min) before Sn precursor injection.

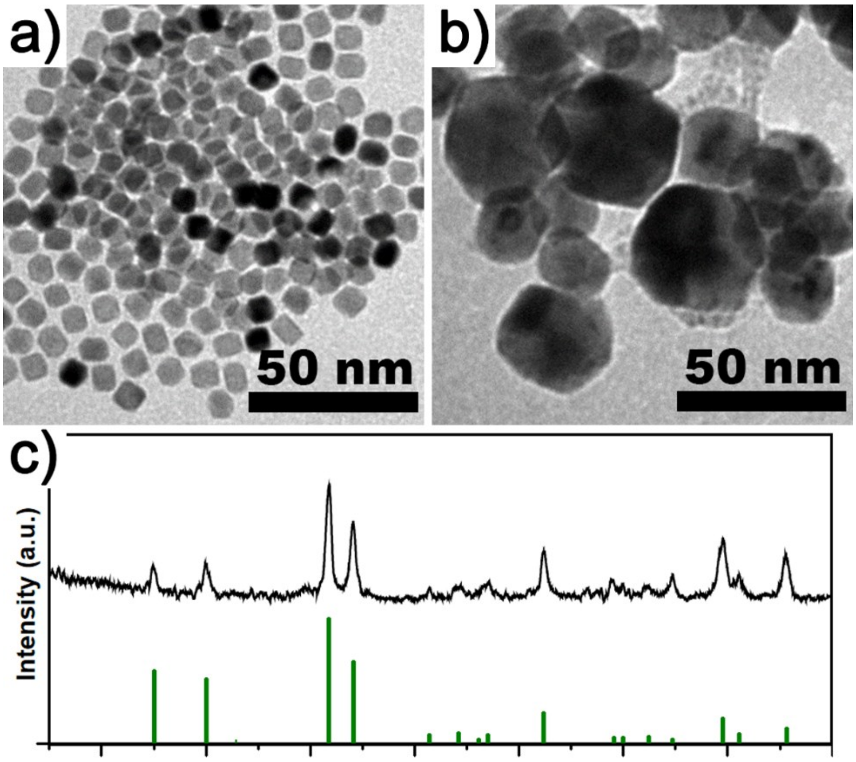

Fig. S14. TEM images of (a) non-dendritic, polyhedral Pt nanocrystals and (b) solid PtSn nanoparticles with Sn precursor injected to the solution containing polyhedral Pt nanocrystals. (c) PXRD pattern of solid PtSn nanoparticles (Fig. S11b) synthesized with spherical Pt nanocrystal and Sn precursor. The green sticks indicate the reference X-ray diffraction lines; PtSn (JCPDS #89-2055)

References for the Supporting Information

[S1] G. Kresse, J. Furthmüller, *Comput. Mater. Sci.*, 1996, **6**, 15.

[S2] G. Kresse, D. Joubert, *Phys. Rev. B*, 1999, **59**, 1758.

[S3] B. Hammer, L. B. Hansen, J. K. Nørskov, *Phys. Rev. B*, 1999, **59**, 7413.

[S4] J. P. Perdew, K. Burke, M. Ernzerhof, *Phys. Rev. Lett.*, 1996, **77**, 3865.

[S5] P. E. Blöchl, *Phys. Rev. B*, 1994, **50**, 17953.

[S6] H. J. Monkhorst, J. D. Pack, *Phys. Rev. B*, 1976, **13**, 5188.